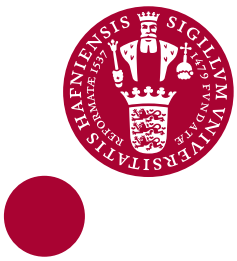

Dietary fat drives whole-body insulin resistance and promotes intestinal inflammation independent of body weight gain

Jensen, Benjamin Anderschou Holbech; Nielsen, Thomas Svava; Fritzen, Andreas Mæchel; Holm, Jacob Bak; Fjære, Even; Serup, Annette Karen Lundbeck; Borkowski, Kamil; Risis, Steve; Pærregaard, Simone I.; Søgaard, Ida; Poupeau, Audrey Angélique G; Poulsen, Michelle; Ma, Tao; Sina, Christian; Kiens, Bente; Madsen, Lise; Kristiansen, Karsten; Treebak, Jonas Thue

Published in:
Metabolism

DOI:
10.1016/j.metabol.2016.09.002

Publication date:
2016

Document version
Publisher's PDF, also known as Version of record

Available online at www.sciencedirect.com

Metabolism

www.metabolismjournal.com

Basic Science

Dietary fat drives whole-body insulin resistance and promotes intestinal inflammation independent of body weight gain

Benjamin A.H. Jensen[a,*], *Thomas S. Nielsen*[b], *Andreas M. Fritzen*[c], *Jacob B. Holm*[a], *Even Fjære*[d], *Annette K. Serup*[c], *Kamil Borkowski*[a], *Steve Risis*[b], *Simone I. Pærregaard*[a], *Ida Søgaard*[a], *Audrey Poupeau*[b], *Michelle Poulsen*[a], *Tao Ma*[a], *Christian Sina*[e], *Bente Kiens*[c], *Lise Madsen*[a,d], *Karsten Kristiansen*[a,f,*], *Jonas T. Treebak*[b,*]

[a] *Laboratory of Genomics and Molecular Biomedicine, Department of Biology, Faculty of Science, University of Copenhagen, Copenhagen, Denmark*

[b] *Novo Nordisk Foundation Center for Basic Metabolic Research, Section of Integrative Physiology, Faculty of Health and Medical Sciences, University of Copenhagen, Copenhagen, Denmark*

[c] *Section of Molecular Physiology, Department of Nutrition, Exercise and Sports, Faculty of Science, University of Copenhagen, Copenhagen, Denmark*

[d] *National Institute of Nutrition and Seafood Research, Bergen, Norway*

[e] *Medical Department, University Hospital Schleswig-Holstein, Campus Lübeck, Germany*

[f] *BGI-Shenzhen, Shenzhen, China*

ARTICLE INFO

Article history:
Received 1 June 2016
Accepted 6 September 2016

Keywords:
Intestinal epithelial cells
Weight stability
Gut microbiota
Feeding behavior
Endogenous glucose production

ABSTRACT

Background. The obesogenic potential of high-fat diets (HFD) in rodents is attenuated when the protein:carbohydrate ratio is increased. However, it is not known if intake of an HFD irrespective of the protein:carbohydrate ratio and in the absence of weight gain, affects glucose homeostasis and the gut microbiota.

Methods. We fed C57BL6/J mice 3 different HFDs with decreasing protein:carbohydrate ratios for 8 weeks and compared the results to a LFD reference group. We analyzed the gut microbiota composition by 16S rDNA amplicon sequencing and the intestinal gene expression by real-time PCR. Whole body glucose homeostasis was evaluated by insulin and glucose tolerance tests as well as by a hyperinsulinemic euglycemic clamp experiment.

Results. Compared with LFD-fed reference mice, HFD-fed mice, irrespective of protein:carbohydrate ratio, exhibited impaired glucose tolerance, whereas no differences were observed during insulin tolerance tests. The hyperinsulinemic euglycemic clamp revealed tissue-specific effects on glucose homeostasis in all HFD-fed groups. HFD-fed mice exhibited decreased insulin-stimulated glucose uptake in white but not in brown adipose tissue, and sustained endogenous glucose production under insulin-stimulated conditions. We observed no impairment of insulin-stimulated glucose uptake in skeletal muscles of different fiber type composition. HFD-feeding altered the gut microbiota composition

* *Corresponding authors.*
E-mail addresses: benjamin.jensen@bio.ku.dk (B.A.H. Jensen), kk@bio.ku.dk (K. Kristiansen), jttreebak@sund.ku.dk (J.T. Treebak).

http://dx.doi.org/10.1016/j.metabol.2016.09.002

paralleled by increased expression of pro-inflammatory cytokines and genes involved in gluconeogenesis in intestinal epithelial cells of the jejunum.

Conclusions. Intake of a HFD profoundly affected glucose homeostasis, gut inflammatory responses, and gut microbiota composition in the absence of fat mass accretion.

1. Introduction

High fat diet-induced obesity is frequently used to study obesity and related metabolic disorders in rodents. Since such a model cannot be used to distinguish whether the observed metabolic dysfunctions result from the obese state or from the high fat feeding, the health consequences of a high fat intake, in the absence of weight gain, remain largely unknown. Using rodent models to elucidate the influence of dietary fat, while eliminating weight gain as confounder, is a challenging approach as high fat diet (HFD)-feeding tends to induce obesity to various degree depending on the protein:carbohydrate ratio [1]. Nevertheless, glucose intolerance induced by conventional HFD-feeding has been shown to precede weight gain in both humans [2] and mice [3], suggesting that a HFD per se affects glucose homeostasis. In support, we have previously demonstrated how exchanging sucrose with casein in an isoenergetic HFD protects against weight gain, but not glucose intolerance [1,4]. The mechanism behind the observed decrease in glucose tolerance remains elusive. Reduced adipose plasticity affecting both local and global insulin signaling [5], and further aggravated by accompanying adipocyte inflammation, may be involved [6]. Yet, whether adipocyte inflammation is a consequence [7] or a promoter [8,9] of insulin resistance remains to be established. Apart from changes in adiposity and adipocyte function, HFDs promote intestinal alterations such as increased intestinal permeability [10] and an elevated inflammatory milieu [11]. Both factors are believed to contribute to the progression of insulin resistance [12]. Interestingly, gut anti-inflammatory agents have been shown to protect against HFD-induced glucose intolerance and insulin resistance despite significant weight gain [13], indicating intestinal inflammation as key in the development of insulin resistance.

We hypothesized that dietary fat, independent of weight gain, would change the intestinal microenvironment translating to impaired metabolic homeostasis. To disentangle the influence of HFD-feeding on intestinal inflammation and whole-body glucose disposal, we fed mice 3 experimental isoenergetic HFDs with fixed fat content and a stepwise increase in the protein:carbohydrate ratio and compared the results to a low fat diet (LFD) reference group. We took advantage of an in-house observation where mice appeared less prone to diet-induced obesity (DIO) in 1 out of our 5 animal facilities, which reflects a recent report deciphering how mouse origin and housing conditions influence weight development [14]. Using the hyperinsulinemic euglycemic clamp technique, this experimental setting enabled acquisition of information on the extent to which macronutrient composition affects whole-body metabolism without possible confounding effects of weight gain and adipose tissue inflammation.

2. Materials and Methods

2.1. Mice and Ethical Statements

Wildtype C57BL/6J male mice (Taconic Biosciences, Denmark) were 6–8 weeks of age at delivery and single-housed for acclimatization one week prior to the start of the experiment. All experiments were conducted in accordance with national Danish guidelines (amendment #1306 of November 23, 2007) as approved by the Danish Animal Experiments Inspectorate (#2014-15-2934-01,027). Mice were kept under specific pathogen free conditions at 22 °C in 12 h light/dark cycle (7 AM–7 PM).

2.2. Experimental Outline and Diets

Twenty-four mice entered the experiment on a weekly basis for 3 consecutive weeks, and mice were kept on their respective diets for 8 weeks. Experimental diets were obtained from Ssniff (Germany) and kept at –20 °C until use. Mice were ad libitum fed 1 of 4 different diets (Table 1): 1) LFD – low fat control diet where sucrose and protein content mirrored the lowest amount in any of the HFDs; 2) HFHP – HFD with normal sucrose but high protein content; 3) HFIP – HFD with intermediate protein and sucrose content; 4) HFNP – HFD with normal protein but high sucrose content. We used corn oil, high in polyunsaturated and low in saturated fat, as fat source to minimize the likelihood of adipose tissue inflammation. Because both protein and carbohydrate sources affect host metabolism, we standardized our diets using casein as protein source and high-glycemic index sucrose as main carbohydrate source. After 5 and 6 weeks on the experimental diets mice were subjected to an insulin tolerance test (ITT)

Table 1 – Diet composition.

MASS (g/kg)	LFD	HFHP	HFIP	HFNP
Casein	200	500	350	200
L-cystine	3	3	3	3
Corn starch	489.5	9.5	9.5	9.5
Cellulose	50	50	50	50
Sucrose	130	130	280	430
Corn oil	70	250	250	250
Choline bitartrate	2.5	2.5	2.5	2.5
Vitamine mix AIN-93-VX	10	10	10	10
Mineral mix AIN 93	45	45	45	45
t-Butylhydroquinone	0.014	0.014	0.014	0.014
Total	1000	1000	1000	1000
Energy content (kJ/kg)	16,972	20,572	20,572	20,572

Diet composition. Comparison between the LF reference diet and the 3 eucaloric HFDs.

and a glucose tolerance test (GTT), respectively. All mice were MR-scanned prior to the ITT using EchoMRI 4in1 (USA). After 7 weeks, a subset of mice in each group underwent a surgical procedure (see Section 2.4. for further details). The remaining mice were used as donor mice to ensure adequate red blood cells (RBCs) during the clamp procedure.

2.3. Insulin/Glucose Tolerance Tests and HOMA-IR

Prior to the ITT and the GTT mice were fasted for 2 h and 5 h, respectively, in clean cages only containing a transparent shelter, bedding and water. Insulin was diluted in succinylated gelatin (Gelofusine® B. Braun Melsungen AG, Germany). Insulin (0.75 U insulin/kg lean mass) and glucose (2 g glucose/kg lean mass) were injected intraperitoneally. Blood glucose was measured in tail vein blood before and 15, 30, 45, 60, 90, and 120 min after the glucose bolus or the insulin bolus, using Contour Next Test Strips (Bayer Contour, USA). HOMA-IR was measured 6 weeks after diet initiation in 5 h fasted mice and calculated as: (fasting plasma glucose (mmol/L) × fasting serum insulin (mU/L))/22.5.

2.4. Hyperinsulinemic Euglycemic Clamp Experiments

The hyperinsulinemic euglycemic clamp was performed in conscious, unrestrained mice. For the surgical catheterization of the jugular vein and the carotid artery, the mice were anesthetized with isoflurane (2.5% for induction, 1.5% for maintenance). Carprofen (10 mg/kg; Rimadyl, Pfizer, USA) was administered preoperatively for analgesia. After surgery, the catheters were locked with heparinized saline (200 U/ml) and the animals recovered for 6 days. Body weight was recorded daily during the recovery period, and mice with a weight loss of more than 10% or a hematocrit level below 35% by day 6 were excluded from the study. On the day of the clamp experiment, mice were fasted for 5 h starting at 7 AM (t = –300 min) by placing them in a clean cage with bedding and nesting material, and free access to water. A divider was placed in the cage restricting the accessible area to ~20 × 20 cm. At t = –180 min the catheters were flushed with heparinized saline (10 U/ml) and the mouse was connected to the infusion lines. A tracer equilibration period was started at t = –90 min by infusion of a 1.2 μCi priming dose of [3-^{3}H]glucose (Perkin Elmer, USA) followed by a constant 0.04 μCi/min infusion of [3-^{3}H]glucose for 90 min. Blood samples for the assessment of hematocrit levels as well as basal glucose levels and turnover rates were collected at t = –15 min (50 μl) and –5 min (100 μl), respectively. The clamp was initiated at t = 0 min with continuous infusions of human insulin (4 mU kg^{-1} min^{-1}; Actrapid, Novo Nordisk, Denmark) and washed red blood cells obtained from a donor mouse to compensate for the blood loss due to repeated sampling (5 μl/min of 50% RBC in 10 U/ml heparinized saline). Blood glucose was measured every 10 min (Bayer Contour, USA) and euglycemia (~5 mmol/L) was maintained by adjusting a variable infusion of 50% glucose containing 0.06 μCi/μl of [3-^{3}H]glucose tracer. Between t = 80 and t = 120 min blood samples (50–100 μl) were collected in 10 min intervals and processed for determination of [3-^{3}H]glucose specific activity. At t = 120 min, a 12 μCi bolus of 2-[1-^{14}C]-deoxy-D-glucose (Perkin Elmer, USA) was injected and blood samples were collected at t = 122, 125, 135, 145, and 155 min, respectively. These samples were processed for determination of 2-[1-^{14}C]-deoxy-D-glucose specific activity. After the final blood sample, mice were euthanized with a lethal dose of pentobarbital and tissues were collected and snap-frozen in liquid nitrogen. The tissues were processed for determination of 2-[1-^{14}C]-deoxy-D-glucose specific activity in order to calculate tissue-specific glucose uptake.

2.5. Clamp Sample Processing and Calculations

Plasma samples were deproteinized with $Ba(OH)_2$ and $ZnSO_4$, and aliquots of each supernatant were transferred to 2 scintillation vials. To determine plasma [3-^{3}H]glucose, one of the aliquots was dried and resuspended in MilliQ water to remove ^3H_2O and the other was counted directly by liquid scintillation counting (Hidex 300 SL). Supernatants for 2-[1-^{14}C]-deoxy-D-glucose determinations were counted directly. Total plasma glucose concentration was determined by adding a reaction mix (200 mmol/L Tris–HCl, 500 mmol/L $MgCl_2$, 5.2 mmol/L ATP, 2.8 mmol/L NADP, and 148 μg of a hexokinase and GPDH mixture (Roche, Germany) pH 7.4) to each sample. Parameters related to glucose turnover rates (R_a, R_d, endoR_a, glycolysis) were calculated as previously described [15]. Tissues were homogenized in ice-cold lysis buffer (pH 7.4, 10% glycerol, 1% IGEPAL, 50 mmol/L Hepes, 150 mmol/L NaCl, 10 mmol/L NaF, 1 mmol/L EDTA, 1 mmol/L EGTA, 20 mmol/L sodium pyrophosphate, 2 mmol/L sodium orthovanadate, 1 mmol/L sodium-pyrophosphate, 5 mmol/L nicotinamide, 4 μmol/L Thiamet G and protease inhibitors (SigmaFast)). Aliquots of each crude homogenate were transferred to two 2 ml tubes and deproteinized with perchloric acid or $Ba(OH)_2$ + $ZnSO_4$. Supernatants were transferred to scintillation vials and counted to determine 2-[1-^{14}C]-deoxy-D-glucose content. Tissue-specific glucose uptake rates were calculated as described previously [16].

2.6. Western Blot Analyses

Approximately 10 mg liver tissue and 25 mg adipose tissue were homogenized (PRECELLYS® 24, USA) in ice-cold lysis buffer (pH 7.4, 10% glycerol, 1% IGEPAL, 50 mmol/L Hepes, 150 mmol/L NaCl, 10 mmol/L NaF, 1 mmol/L EDTA, 1 mmol/L EGTA, 20 mmol/L sodium pyrophosphate, 2 mmol/L sodium orthovanadate, 1 mmol/L sodium-pyrophosphate, 5 mmol/L nicotinamide, 4 μmol/L Thiamet G and protease inhibitors (SigmaFast, Sigma-Aldrich, USA)). Homogenates were incubated end-over-end for 45 min (4 °C), followed by centrifugation at 16,000g for 10 min (4 °C). Supernatants were stored in aliquots at –80 °C until further analysis. Protein concentration was measured by BCA (#23,223 and #23,224, Thermo Scientific, USA) according to the manufacturer's instructions. Western blot analyses were performed as previously described [17] using the following antibodies: anti-ACCβ Ser^{79} phosphorylation (#07-303, Upstate Biotechnology, USA), anti-AKT Thr^{308} phosphorylation (#9275, Cell Signaling Technologies, USA), anti-AKT Thr^{473} phosphorylation (#9271, Cell Signaling Technologies, USA), anti-AKT 2 (#3063, Cell Signaling Technologies, USA).

2.7. Isolation of Intestinal Epithelial Cells (IECs)

The small intestine was sectioned in 8 equal segments. The 5th and the 8th segments, starting from duodenum, were

collected as representative of the jejunum and the ileum [18] for isolation of the intestinal epithelial cells. These segments were flushed with cold PBS buffer, cut open in the length and fractioned in 0.2–0.5 cm pieces. Samples were placed on ice and separately incubated in 5 ml of buffer (Matrisperse cell recovery solution, Corning, USA) for 40 min allowing epithelium detachment [19,20]. Efficient recovery of crypt and villi and viability of the epithelial cells were controlled on a microscope following a trypan blue (Sigma-Aldrich, USA) staining. Cells were centrifuged at 10,000*g* for 2 min and snap frozen in liquid nitrogen. Total RNA was extracted with TRIzol reagent (Invitrogen, USA), and RNA quality was assessed on a Bioanalyzer (Agilent, USA) by RIN value (28S/18S ratio). Samples with a RIN value below 7 were excluded.

2.8. Quantitative PCR

Total RNA of adipose tissues was extracted by TRIreagent® (Sigma-Aldrich, USA) according to manufacturer's protocol using PRECELLYS® 24 for homogenization. One microgram of RNA was transcribed into cDNA by reverse transcriptase (Invitrogen, USA). Quantitative PCR analyses were performed using the SYBR Green qPCR Master mix (Thermo Scientific, USA) and the Stratagene Mx3000P qPCR System. Primer sequences are summarized in Supplementary Table S1.

2.9. 16S rDNA Amplicon Sequencing and Bioinformatics

Bacterial DNA from cecal and colon samples was extracted using a NucleoSpin soil kit (Macherey-Nagel, Germany) according to manufacturer's instructions. DNA yield and integrity were assessed using a Nanodrop (Thermo Scientific, USA) and agarose gel electrophoresis, respectively. PCR-based library formation targeting the 16S rRNA gene's variable region 4 (V4) was performed as previously described [21]. The PCR products were purified using Agencourt AMPure XP (Beckman Coulter, USA) beads and pooled in equal concentrations. Sequencing was performed using an Illumina MiSeq with V2 PE500 cartridge (500 cycles). The generated data was analyzed using QIIME [22] v1.9.1 with default settings. UCHIME [23] was used for chimera checking and UCLUST [24] for de novo OTU-picking based on 97% sequence similarity. Bacterial taxonomy was assigned using the RDP-classifier [25] and Greengenes [26] database v13.8. Subsequent analysis was performed in R v3.2.3 using the Phyloseq [27], metagenomeSeq [28] and Vegan [29]. Low-abundance operational taxonomic units (OTUs) were filtered from the data by removal of OTUs present in fewer than 3 of the samples or with a relative abundance across all samples of less than 0.005%. The data used for the analysis contained on average 18.494 ± 3.422 (SD) sequences per sample after filtering. Analysis of bacterial differential abundance was performed on data normalized with metagenomeSeq using cumulative-sum scaling. In addition, the statistical analyses using metagenomeSeq were performed on data filtered based on effective sample sizes, where taxa were not included if they had fewer than X effective number of positive samples, where X is the median of estimated effective samples per feature.

2.10. Histology Examination and Adipose Tissue Histology

Liver and adipose tissues were fixed in 4% phosphate buffered paraformaldehyde, dehydrated, and paraffin embedded. Five micrometer sections from 6 to 8 mice of epididymal white adipose tissue (eWAT) and inguinal white adipose tissue (iWAT) were stained with hematoxylin and eosin (H&E). One representative micrograph of each group is shown, and 2 sections of adipose tissue depots from each mouse were measured by drawing and used for quantification of mean cell diameter using Image J open source software.

2.11. Histopathological and Immunohistochemical Analysis of Mouse Liver Tissue

Preparation of liver sections and histopathological techniques were performed according to standard protocols. Two independent observers performed all histological assessments in a blinded fashion. We used the established NAFLD activity score (NAS) for evaluation of H&E stained random liver sections as described elsewhere [30]. Briefly, a score of 0 to 2 excludes non-alcoholic steatohepatitis (NASH), a score of 3–4 defines "borderline NASH", whereas a score of 5 and higher assures the full picture of NASH.

2.12. Lipid Profile and Thin-Layer Chromatography

Diacylglycerol (DAG) and triacylglycerol (TAG) were measured on 5 mg liver and ceramide content was measured on 20 mg liver by thin-layer chromatography (TLC). Lipids were extracted in chloroform–methanol (2:1) [31] and dissolved in chloroform as previously described [32]. DAG, TAG, and ceramides were separated on silica-gel coated plates using two different separate mobile phases consisting of chloroform–methanol–acetic acid–water (50:50:5:5) followed by petroleum ether–diethyl ether–acetic acid (120:25:1.5) for DAG and TAG and chloroform–methanol–acetic acid (98:2:0.5) for ceramides. Butylated hydroxytoluene (50 mg/L) was added to both of the mobile phases. The lipids were developed by a 10% copper sulfate pentahydrate and 8% phosphoric acid solution at 120 °C for 15 min for DAG and TAG and at 140 °C for 10 min for ceramides. The silica coated plates were visualized on a Typhoon FLA 7000 IP fluorescent scanner and analyzed according to weight using ImageQuant TL (GE Healthcare Life sciences, United Kingdom).

2.13. Immuno Assays

Plasma insulin, adiponectin, and tumor necrosis factor alpha (TNF-α) were analyzed on the MSD platform (Mesoscale, USA), while serum amyloid A (SAA) was analyzed by standard ELISA (Abcam, USA) according to the manufacturers' protocol.

2.14. Statistical Analyses

Data are presented as mean ± SEM. All time-dependent analyses were evaluated by two-way repeated measures (RM) ANOVA, Dunnett post hoc test. Time-independent

analyses were evaluated by one-way ANOVA, Dunnett post hoc test. Bacterial composition was examined using the metagenomeSeq package and adonis test in R and correlation analyses were examined by Spearman rank correlation test, adjusted for multiple comparisons by Benjamin and Hochberg false discovery rate (FDR) test. qPCR data on IECs were log (Ln) transformed prior statistical analyses due to a non-Gaussian distribution. Statistical significance was set at $p < 0.05$ and the different levels of significance were set at $^{*} = p < 0.05$, $^{**} = p < 0.01$, $^{***} = p < 0.001$.

3. Results

3.1. *High-Fat Diets Induce Glucose Intolerance Independent of Protein and Sucrose Content*

We used 3 isoenergetic HFDs designated HFHP, HFIP and HFNP with matched fat content (45% energy from fat) and a stepwise increased protein:carbohydrate ratio, and compared the results to a LFD reference group. To determine the influence of dietary

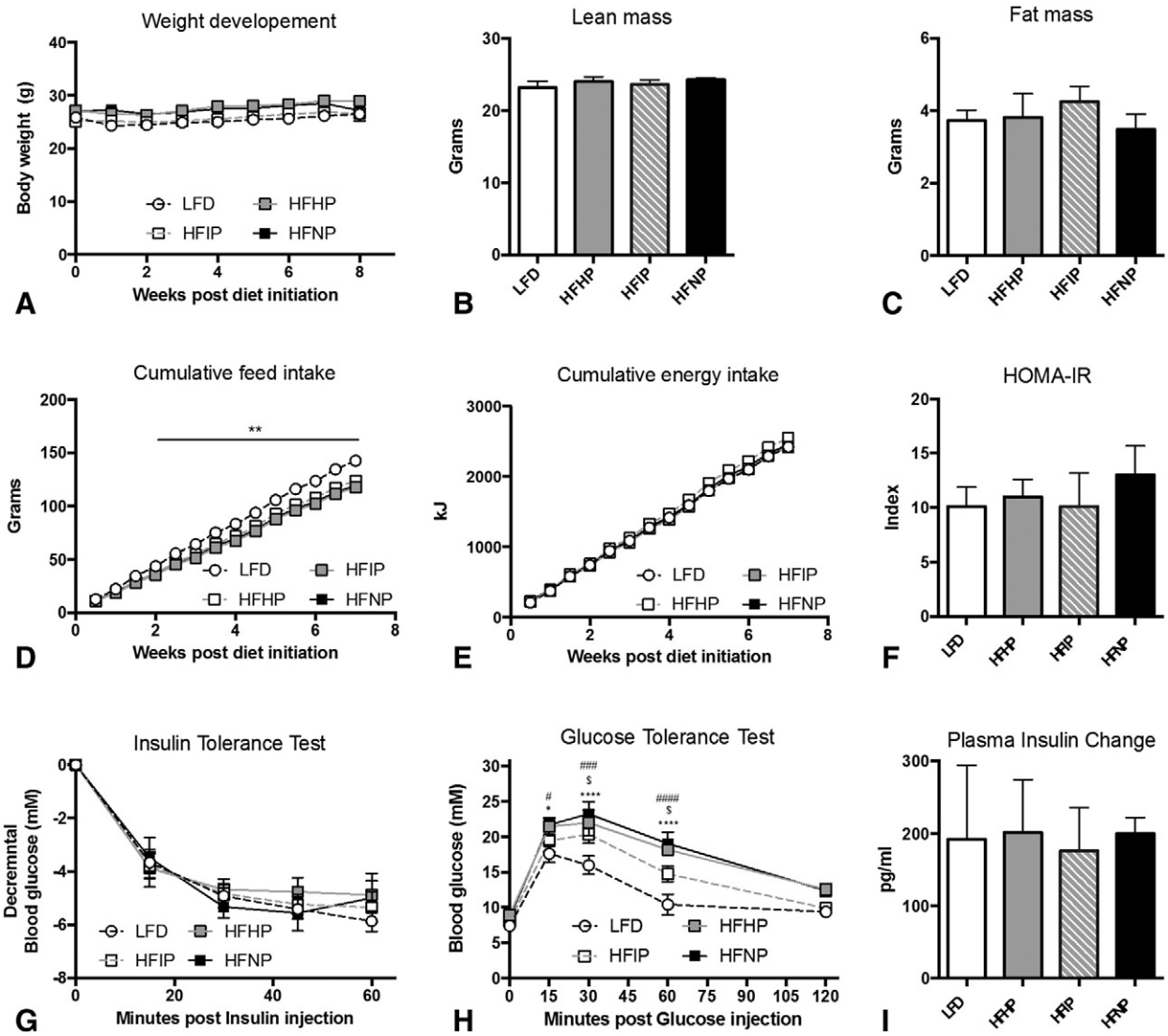

Fig. 1 – High-fat diets induce glucose intolerance independently of background diet and obesity. 8-week-old male mice were fed either a high-fat-high-protein (HFHP), a high-fat-intermediate-protein (HFIP) or a high-fat-normal-protein (HFNP) diet for 8 weeks. A) Body weight development. B) Lean body mass 5 weeks post diet initiation. C) Fat mass 5 weeks post diet initiation. D) and E) feed consumption. F) HOMA-IR 6 weeks post diet initiation. G) Insulin tolerance test 5 weeks post diet initiation. H) Glucose tolerance test 6 weeks post diet initiation. I) Plasma insulin change from prior to 5 min after a glucose bolus in 5-h fasted mice. Data are presented as mean ± SEM. *n* = 6 mice per group. A–E, G–H: One representative out of 3 independent experiments. F and I: One representative out of 2 independent experiments. 1- and 2-way ANOVA where appropriate, Dunnett post hoc test. In H: # indicates difference between HFHP and LFD; $ indicates difference between HFIP and LFD, * indicates difference between HFNP and LFD.

fat, carbohydrate, and protein, we used an animal facility where mice empirically are known to be less prone to DIO. Accordingly, body weight and fat composition were similar between groups (Fig. 1A–C). LFD-fed mice had a higher feed intake (grams of feed consumed) than HFD-fed mice. This was most likely a consequence of a less energy dense diet (Table 1), as the calorie intake was similar between the groups (Fig. 1D and E, respectively). These findings were replicated in 3 independent experiments ($n = 6$). In this experimental setting, we were able to obtain information on the extent to which macronutrient composition affected whole-body metabolism without confounding effects of weight gain. Compared to LFD reference mice, 5 weeks of HFD feeding did not affect the blood glucose response to a single insulin bolus regardless of the protein:carbohydrate ratio (Fig. 1G). However, all HFD-fed groups had reduced glucose tolerance by 6 weeks of HFD feeding (Fig. 1H), suggesting that HFDs impaired glucose homeostasis independent of weight gain and protein:carbohydrate ratio. The observed discrepancy between glucose intolerance (Fig. 1H) and systemic insulin sensitivity (Fig. 1F–G) could indicate impaired insulin secretion capacity. However, glucose-stimulated insulin secretion measured 5 min post glucose bolus was indistinguishable between groups (Fig. 1I).

3.2. *Intestinal Alterations in the Microbiome Potentially Translate to Increased Gluconeogenesis in the Small Intestine of HFD-Fed Mice*

The difference between glucose tolerance and insulin sensitivity prompted us to investigate whether alterations in the gut might be involved. A possible scenario would involve diet-dependent alterations in the composition of the gut microbiota, which subsequently could affect intestinal gene expression disturbing metabolic homeostasis. Consequently, we analyzed the intestinal microbiota composition based on 16S rDNA amplicon sequencing. We observed a pronounced separation between the colonic and cecal microbiota in all HFD-fed mice and the LFD-fed reference mice (Figs. 2A–C and S1A–C). Among the HFD-fed mice only the HFHP and HFIP groups separated significantly (adonis unweighted unifrac $p = 0.023$). A higher relative abundance of a single family, namely S24-7 from the Bacteroidetes phylum was the main difference comparing the HFHP with the HFIP group (Figs. 2D and S1D). Despite the observed changes in the S24-7 abundance, our data strongly suggest that in these settings, dietary fat is a stronger driver of alterations in the composition of the gut microbiota than the amount and/or ratio between dietary carbohydrate and protein.

Intestinal epithelial cells (IECs) are 'first line responders' to dietary constituents and key in intestinal gluconeogenesis [33]. Intestinal gluconeogenesis accounts for up to 20% of host glucose production [34] and can therefore significantly affect host glucose homeostasis [35,36]. Moreover, IECs have immune modulatory potential [37] releasing pro-inflammatory cytokines to the portal circulation, thereby potentially aggravating hepatic insulin resistance. We therefore analyzed gene expression in ileal and jejunal IECs. Compared to the LFD-fed reference mice, we observed significant induction of expression of *Nos2*, *Tnfa*, and *Il23a* in the jejunum of HFHP fed mice, whereas mice fed the HFNP diet exhibited induction of *Nos2* and *Il1b*. In contrast, expression of *Il10* and *Il13* tended to decrease in mice fed either of the HFDs. In the ileum, no significant changes in expression of these cytokines were observed (Fig. 2E–F). Interestingly, in all HFD-fed mice, irrespective of the ratio between carbohydrate and protein, we observed a striking induction of *Pck1* and *G6pc* both in the jejunum and the ileum (Fig. 2H), suggesting that increased intestinal gluconeogenesis may contribute to the observed impaired glucose tolerance.

3.3. *Protein:Carbohydrate Ratio Modulates Liver Histology*

To further investigate possible mechanisms contributing to the observed impaired glucose tolerance, we investigated whether cytokines released from the intestine had affected liver metabolism, including accumulation of lipids. None of the HFD-fed mice exhibited ectopic lipid accumulation as determined by analysis of hepatic levels of TAG, DAG, and ceramides (Fig. 3A). Furthermore, serum amyloid A, an acute phase protein with high dynamic range, primarily reflecting hepatic secretion, and a potential biomarker of insulin resistance [38], did not differ between groups (Fig. S2a). However, immunohistochemical analyses revealed a borderline increase in the NAFLD activity score in mice fed the HFNP diet (Fig. 3B–C). This finding suggested that the protein:carbohydrate ratio in connection with HF-feeding may affect hepatic metabolism in a manner not detectable by biochemical analysis of lipid accumulation, and that the HFDs with high and intermediate protein:carbohydrate ratio counteracted this increase in the NAFLD activity score.

3.4. *Tissue-Specific Alterations in Insulin-Stimulated Glucose Uptake in Response to HFD Feeding*

To further examine the metabolic alterations associated with the HFD-feeding, we determined whole-body insulin sensitivity and tissue-specific insulin-stimulated glucose uptake by performing a hyperinsulinemic euglycemic clamp experiment in cohorts of mice challenged by the 4 different diets (Fig. 4A). In parallel to the decreased glucose tolerance observed during GTT, the glucose infusion rate under insulin-stimulated conditions (Fig. 4B) was decreased in all HFD-fed mice compared to LFD-fed reference mice. This observation was marginally different under steady state conditions (Fig. 4C), where only HFHP and HFIP reached the level of statistical significance. For glucose disappearance rate (Fig. 4D), only the HFIP group was significantly different from the LFD reference mice, albeit all HFD-fed mice trended towards decreased glucose disappearance. All HFD-fed groups appeared to have sustained EGP under clamped condition (Fig. 4E), indicating decreased insulin-mediated suppression of gluconeogenesis. The apparently sustained EGP was, however, not significantly different from the LFD reference group, presumably due to insufficient power ($n = 4$–7 mice per group). Still, sustained EGP was unlikely to be the only mechanism behind the observed glucose intolerance. Accordingly, we examined insulin-stimulated glucose disposal in peripheral tissues. Irrespective of the diet composition, clamped mice had comparable insulin-stimulated glucose uptake in soleus, extensor digitorum longus (EDL), and tibialis anterior (TA) muscles (Fig. 4F). However, we observed a significant

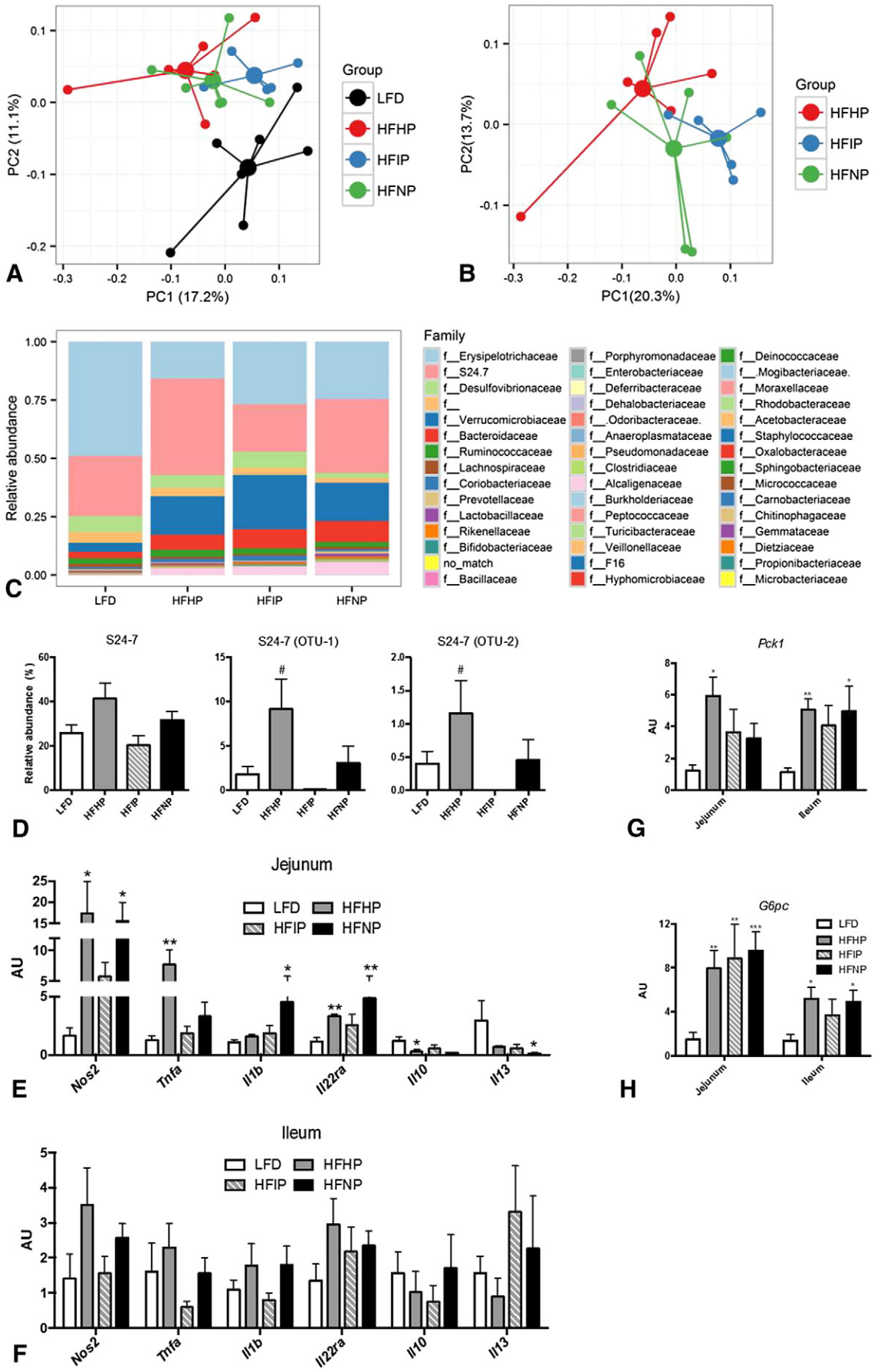
A
PC2 (11.1%)
PC1 (17.2%)
Group
LFD
HFHP
HFIP
HFNP
B
PC2(13.7%)
PC1(20.3%)
Group
HFHP
HFIP
HFNP
C
Relative abundance
LFD
HFHP
HFIP
HFNP
Family
f__Erysipelotrichaceae
f__S24.7
f__Desulfovibrionaceae
f__Verrucomicrobiaceae
f__Bacteroidaceae
f__Ruminococcaceae
f__Lachnospiraceae
f__Coriobacteriaceae
f__Prevotellaceae
f__Lactobacillaceae
f__Rikenellaceae
f__Bifidobacteriaceae
no_match
f__Bacillaceae
f__Porphyromonadaceae
f__Enterobacteriaceae
f__Deferribacteriaceae
f__Dehalobacteriaceae
f__.Odoribacteraceae.
f__Anaeroplasmataceae
f__Pseudomonadaceae
f__Clostridiaceae
f__Alcaligenaceae
f__Burkholderiaceae
f__Peptococcaceae
f__Turicibacteraceae
f__Veillonellaceae
f__F16
f__Hyphomicrobiaceae
f__Deinococcaceae
f__.Mogibacteriaceae.
f__Moraxellaceae
f__Rhodobacteraceae
f__Acetobacteraceae
f__Staphylococcaceae
f__Oxalobacteraceae
f__Sphingobacteriaceae
f__Micrococcaceae
f__Carnobacteriaceae
f__Chitinophagaceae
f__Gemmataceae
f__Dietziaceae
f__Propionibacteriaceae
f__Microbacteriaceae
D
S24-7
S24-7 (OTU-1)
S24-7 (OTU-2)
Relative abundance (%)
LFD
HFHP
HFIP
HFNP
G
Pck1
AU
Jejunum
Ileum
E
Jejunum
LFD
HFHP
HFIP
HFNP
AU
Nos2
Tnfa
Il1b
Il22ra
Il10
Il13
H
G6pc
AU
Jejunum
Ileum
F
Ileum
LFD
HFHP
HFIP
HFNP
AU
Nos2
Tnfa
Il1b
Il22ra
Il10
Il13

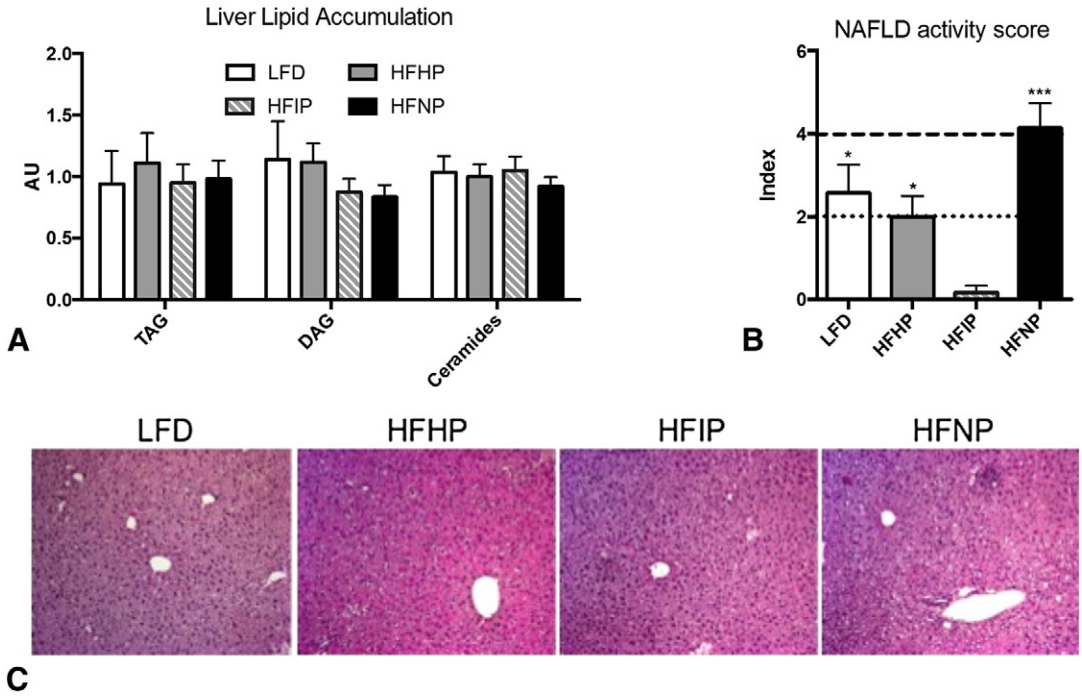

Fig. 3 – The dietary protein:carbohydrate ratio affects NAFLD development. Mice were fed experimental diets for 8 weeks before tissues were either fixed in paraformaldehyde and prepared for paraffin embedding, or snap frozen in liquid nitrogen. All mice were euthanized in the morning. They had free access to feed. A) Hepatic lipid accumulation. B) NAFLD activity score evaluated by inspection of images from C. C) H&E stains of lever sections, one representative out of 4–6 images per group. A–B: Data are represented as mean ± SEM. 1-way ANOVA, Tukey post hoc test. * depicts difference between the labeled group and the HFIP-fed group. *n* = 6–8 mice per group.

decrease in insulin-stimulated glucose uptake in iWAT of all HFD-fed mice compared to LFD reference mice, and a tendency to decreased glucose uptake in eWAT, but no intergroup variation in brown adipose tissue of clamped mice (Fig. 4G).

3.5. *Insulin Signaling is Impaired in iWAT of HFD Fed Mice*

The above results prompted us to investigate adipose tissue morphology and function. All HFD-fed groups displayed enlarged adipocytes in both eWAT and iWAT (Fig. 5A–B) despite a lean phenotype and uniform fat mass between groups. Serum fatty acids and TAG concentrations were not altered between groups; neither under basal nor clamped conditions (Fig. S2D–E). In keeping with the marked decrease in glucose uptake particularly in iWAT, we focused our subsequent analyses on this depot.

AKT phosphorylation at Thr308 and Ser473 under insulin-stimulated conditions did not differ between groups when the statistical analyses were run on data from each phosphorylation site separately (Fig. 5C). However, performing a two-way ANOVA on the combined data from both phosphorylation sites revealed a significant main effect of "diet" ($p = 0.028$), and subsequent posthoc tests using the Dunnett's method with the LFD group as control group showed a significant difference between LFD and the HFNP groups ($p = 0.021$), and borderline significant differences between LFD and HFHP ($p = 0.055$) and LFD and HFIP ($p = 0.068$). Thus, effects of insulin on AKT signaling are generally reduced in all HFD-fed groups.

Fig. 2 – Intestinal alterations in HFD-fed mice affect expression of genes involved in gluconeogenesis in the small intestine. A) Principle Component Analysis (PCoA) plot using unweighted Unifrac distance. The colonic microbiome of all HFD-fed mice differed significantly from that of the LFD control group (adonis test: $p < 0.05$). B) As in A, except here only the HFD-fed mice are depicted allowing better separation of the experimental diets. The microbiome composition of colonic samples from the HFHP and HFIP fed mice differed significantly from each other (adonis test: $p = 0.023$). C) Taxa summary plot of relative abundance of microbial communities at the family level in the colonic samples. D) Relative abundance of the bacterial family S24-7 and the two OTUs with the highest relative abundance found to differ significantly between mice fed the HFHP and HFIP diets. E) Inflammatory gene expression profile in IECs of jejunum. F) As in E except this panel shows the gene expression in IECs of ileum. G) and H) Gene expression of gluconeogenic genes in jejunum and ileum. D–H: Data are presented as mean ± SEM. 1-way ANOVA, Dunnett post hoc test. * indicates difference between the labeled group and LFD reference group, # indicates different from the HFIP group (*n* = 5–8 mice per group).

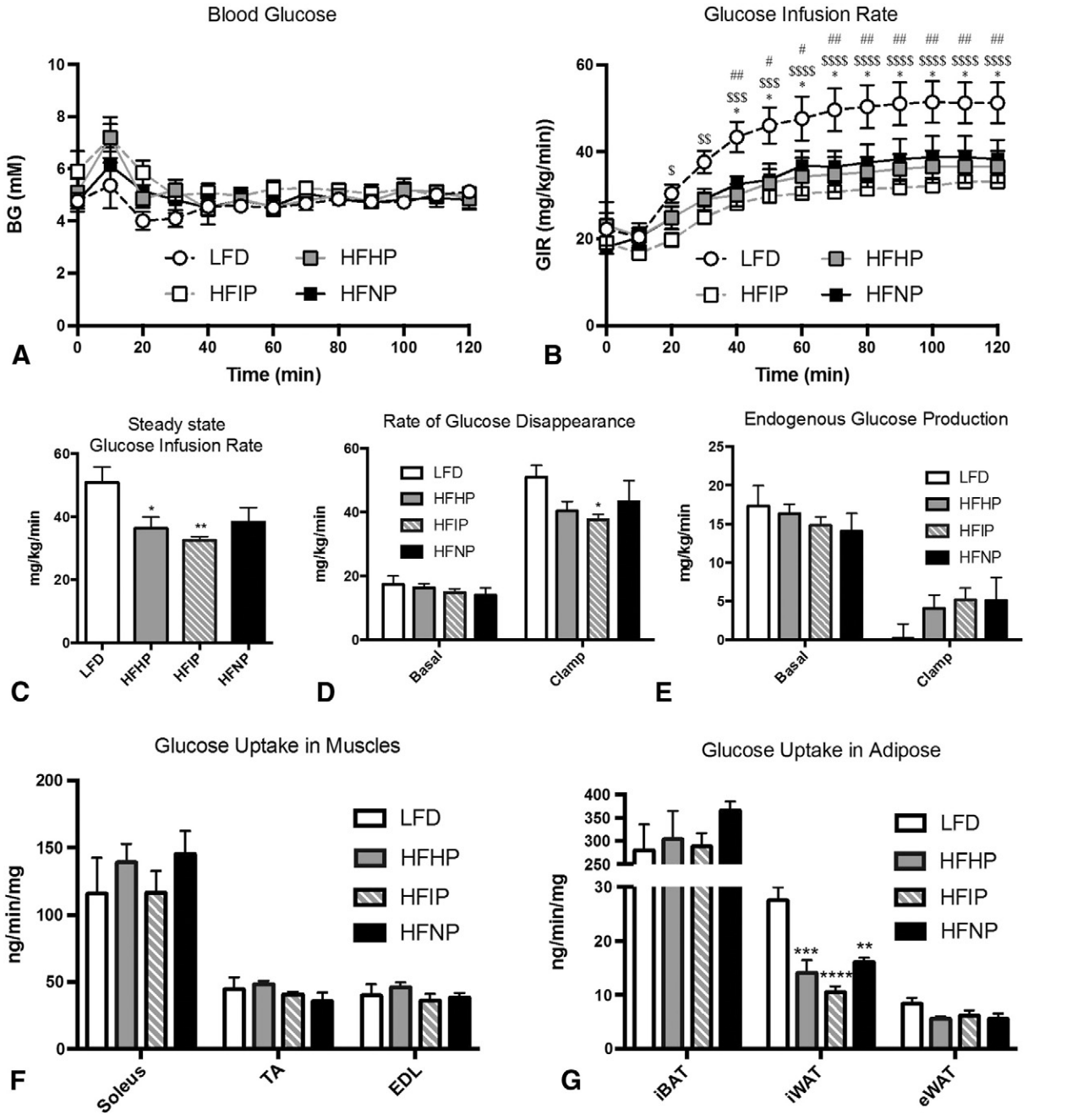

Fig. 4 – Hyperinsulinemic euglycemic clamp reveals tissue-specific alterations in insulin-stimulated glucose uptake in response to HFD. Mice were fed experimental diets for 7 weeks before insertion of catheters into the jugular vein and carotid artery, respectively. After surgery, mice were allowed to recover for 6 days before the clamp. A) Blood glucose during the two-hour clamp. B) Glucose infusion rate needed to stabilize blood glucose level (A) under continuous and fixed insulin infusion. C) Steady state glucose infusion rate. D) Rate of glucose disappearance before and during clamp. E) Hepatic glucose production before and during clamp. F) Insulin-stimulated glucose uptake in muscles. G) Insulin-stimulated glucose uptake in adipose tissue. Data are presented as mean ± SEM. *n* = 4–7 mice per group. 1- and 2-way ANOVA where appropriate, Dunnett post hoc test. In B: # indicates difference between HFHP and LFD; $ indicates difference between HFIP and LFD, * indicates difference between HFNP and LFD. In all other panels: * indicates difference between labeled column and LFD. TA: tibialis anterior, EDL: extensor digitorum longus.

Reduced AMP-activated protein kinase (AMPK) activity in WAT has been linked to insulin resistance in humans [39], and acetyl-CoA carboxylase (ACC) phosphorylation mirrors AMPK activity in both muscles and adipose tissue [40,41]. We found significantly decreased phosphorylation of ACC at Ser79 ($p = 0.0015$ and $p = 0.0017$, respectively, Fig. 5D) in HFHP- and HFIP-fed mice, suggesting a decreased activity of AMPK in iWAT of HFHP- and HFIP-fed mice.

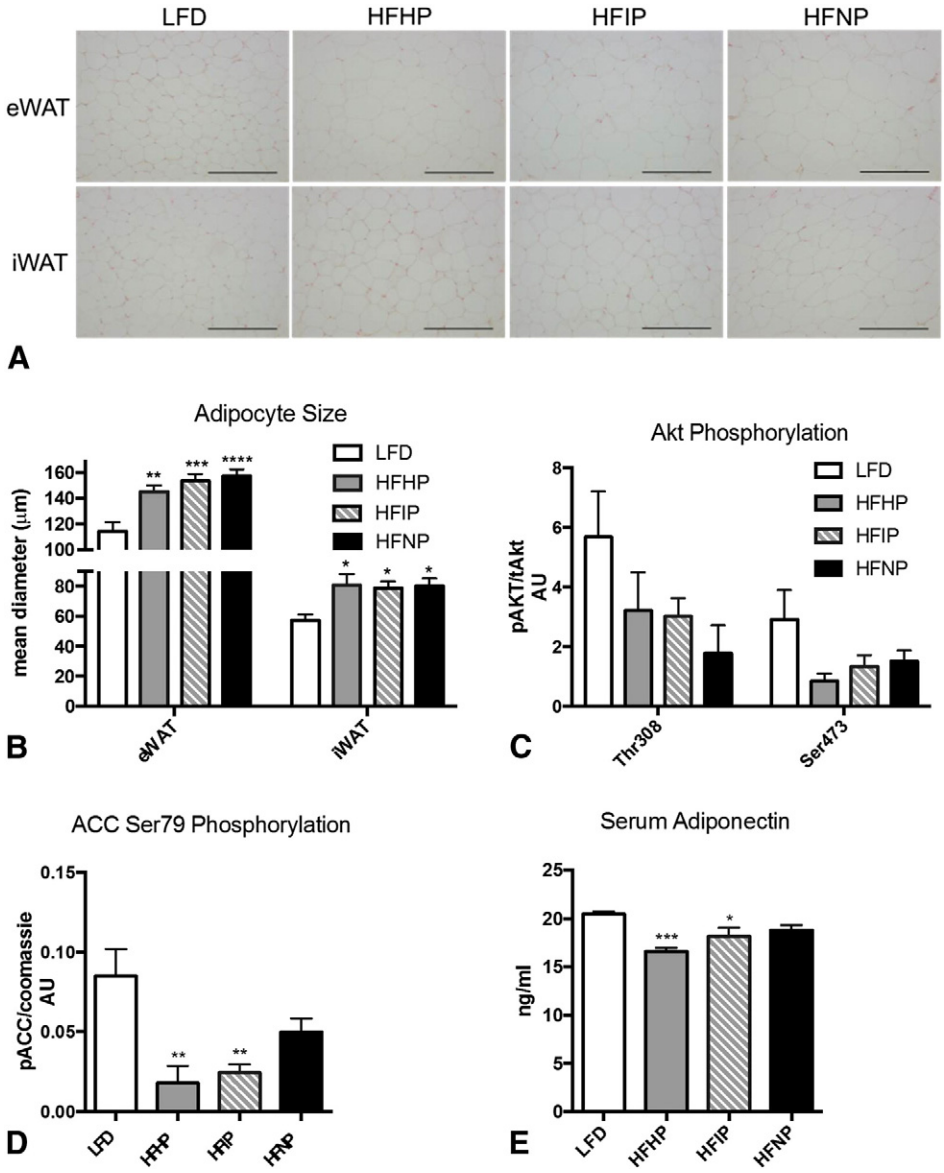

Fig. 5 – Insulin signaling is impaired in iWAT of HFD-fed mice. Mice were fed experimental diets for 8 weeks before tissues were either fixed in paraformaldehyde and prepared for paraffin embedding or snap frozen in liquid nitrogen. All mice were euthanized in the morning. They had free access to feed. A) Histology section of paraffin embedded WAT. B) Adipocyte size as visualized in A. C) and D) phosphorylation of AKT and ACC, respectively. E) Serum adiponectin. In B–E: Data are presented as mean ± SEM. n = 5–8 mice per group. 1-way ANOVA, Dunnett post hoc test. * indicates difference between labeled column and LFD. In C: As a measure of a general effect of AKT phosphorylation a 2-way ANOVA, Dunnett post hoc test was performed. The HFDs were compared to the LFD reference group an adjusted for multiple comparisons showing a main effect on AKT phosphorylation in HFNP-fed mice (HFHP: p = 0.0547; HFIP: p = 0.0848; HFNP: p = 0.0205).

Adiponectin is an insulin-enhancing adipokine [42] exerting both autocrine and paracrine functions. At the autocrine level, adiponectin stimulates lipid storage and enhances both insulin-stimulated glucose uptake [43] and AMPK activation [44]. HFHP- and HFIP-fed mice had reduced levels of circulating adiponectin compared to LFD reference mice, while HFNP-fed mice only trended towards a reduction in serum adiponectin (Fig. 5E). Interestingly, the pro-inflammatory cytokine, TNF-α, has been shown to induce a lowering of adiponectin release in adipose tissue of lean, but not obese individuals [45]. As neither circulating TNF-α protein nor WAT mRNA levels of *Tnfa* (Fig. S2B and C–D, respectively) were different between LFD and HFD-fed groups, TNF-α may not explain the observed reduced adiponectin levels. Inspection of H&E stained tissue sections revealed no increase in macrophage infiltration and crown like structures (CLSs) into white adipose tissue (data not shown), and we did not observe alterations in mRNA expression of macrophage chemo-attractant protein-1 (*Mcp-1*), or the inflammatory regulators, interleukin (*Il*)*1b* and *Il6* (Fig. S2C–D). Finally, we asked if the serum protein levels of another macrophage chemo-attractant, C-X-C motif chemokine 10 (CXCL10), an anti-inflammatory molecule, IL10, as well as

Table 2 – Spearman correlation analysis.

Variable 1	Variable 2	r	p
Fat	Weight change	0.39	0.035
Fat	Adipocyte size, eWAT	0.32	0.009
Fat	*G6pc*, jejunum	0.32	0.008
Fat	Serum adiponectin	–0.47	0.033
Protein	Serum adiponectin	–0.54	0.012
Carbohydrate (sucrose)	*Il13*, jejunum	–0.51	0.025
Weight change	*Pck1*, jejunum	0.47	0.041
Adipocyte size, eWAT	*Il10*, jejunum	–0.54	0.021
Adipocyte size, iWAT	Adipocyte size, eWAT	0.71	0.00032
Adipocyte size, iWAT	*Nos2*, jejunum	0.52	0.033
Adipocyte size, iWAT	*Pck1*, jejunum	0.56	0.018
Adipocyte size, iWAT	*G6pc*, jejunum	0.58	0.015
iNOS, jejunum	*Il1β*, jejunum	0.69	0.001
iNOS, jejunum	*Il22r*, jejunum	0.57	0.011
iNOS, jejunum	*Pck1*, jejunum	0.61	0.005
iNOS, jejunum	*G6pc*, jejunum	0.53	0.19
IL-1β, jejunum	*Il22r*, jejunum	0.64	0.003
IL-1β, jejunum	*Pck1*, jejunum	0.48	0.038
IL-1β, jejunum	*G6pc*, jejunum	0.46	0.045
IL-22r, jejunum	*Pck1*, jejunum	0.46	0.049
IL-22r, jejunum	*G6pc*, jejunum	0.56	0.013
IL-22r, jejunum	Serum adiponectin	–0.53	0.019
Serum adiponectin	*Il10*, jejunum	0.48	0.038
Serum adiponectin	*Il22r*, jejunum	–0.53	0.019

The following variables were compared: 1) inflammatory gene expression in jejunum. 2) Gluconeogenic gene expression in jejunum. 3) Serum adiponectin. 4) Weight change. 5) Adipozyte size of iWAT and eWAT. 6) Sucrose, fat, and protein intake. Only correlations that met the criteria of $p < 0.05$ and $r \geq 0.3$ with a subsequent FDR <0.05 are depicted. n = 17–19 per correlation.

resistin were altered between HFD-fed mice and LFD reference mice. Both resistin and CXCL10 have been reported to be increased in human type 2 diabetic patients [46,47], whereas serum IL10 levels appear to be decreased in type 2 diabetic patients [48]. However, none of these markers differed between the four groups of mice (Fig. S2B).

3.6. *Dietary Fat is a Predominant Driver of Diet-Induced Immuno-Metabolic Alterations*

Investigating the correlation between jejunal gene expression, adipocyte size, adiponectin secretion and weight change by Spearman correlation analysis indicated a correlation between intestinal inflammatory profile and expression of gluconeogenic genes (Table 2). Bridging intestinal immunity to whole-body metabolism, the inducible isoform of nitric oxide synthases, NOS2, involved in pro-inflammatory immune responses, was found to positively correlate with adipocyte size in iWAT (Table 2, $r = 0.52$, $p = 0.033$), whereas the anti-inflammatory cytokine IL10 correlated negatively with adipocyte size in eWAT (Table 2, $r = –0.54$, $p = 0.021$). Spearman correlation analyses including dietary constituents revealed fat as the most prominent driver, correlating positively with weight change (Table 2, $r = 0.39$, $p = 0.035$), adipocyte size in eWAT (Table 2, $r = 0.32$, $p = 0.009$), and also with jejunal *G6pc* expression (Table 2, $r = 0.32$, $p = 0.008$), while correlating negatively with serum adiponectin (Table 2, $r = –0.47$, $p = 0.033$). Sucrose was inversely correlated with jejunal transcripts of *Il13* (Table 2, $r = –0.51$, $p = 0.021$), and protein intake was, like fat intake, inversely correlated with serum adiponectin (Table 2, $r = –0.54$, $p = 0.012$). Interestingly, serum adiponectin levels were not correlated with expression of markers for intestinal gluconeogenesis (*Pck1*: $r = –0.27$, $p = 0.257$; *G6pc*: $r = –0.33$, $p = 0.166$) or adipocyte size, albeit a borderline correlation between serum adiponectin and eWAT cell size ($p = 0.053$, $n = 18$) but not iWAT cell size ($p = 0.204$, $n = 17$) was observed. In contrast, adipocyte size correlated with both inflammatory and gluconeogenic jejunum gene expression (Table 2).

4. Discussion

In the present study we demonstrate that HFD consumption impaired whole-body glucose homeostasis independent of weight gain and irrespective of the protein:carbohydrate ratio. The observed glucose intolerance of HFD-fed animals may be a consequence of elevated gluconeogenic potential in intestinal epithelial cell which is supported by our finding of increased expression of gluconeogenic genes in the epithelial cells of the jejunum and ileum, and the sustained EGP during the hyperinsulinemic euglycemic clamp experiments in these animals. We did not observe any impairment of glucose-stimulated insulin secretion as measured 5 min after administration of a glucose bolus, and inflammation markers in adipose tissues were not elevated. However, insulin-stimulated glucose uptake in iWAT was impaired and was accompanied by decreased insulin-dependent phosphorylation of AKT. Collectively, our data support that diminished insulin-dependent glucose uptake in adipose tissues and increased intestinal gluconeogenesis contribute to the observed impaired glucose tolerance.

Diets high in protein have been suggested to promote leanness through increased satiety mediated by an augmented intestinal gluconeogenesis [36]. Yet, we did not find changes in gene expression of gluconeogenic genes, or changes in feed intake as a function of dietary protein content. Rather, we observed that induction of key genes involved in intestinal gluconeogenesis correlated with high fat intake. Dietary fat intake has previously been found to be a more powerful driver of changes in the composition of the gut microbiota than the protein:carbohydrate ratio [49]. Our analyses confirm this finding and further show that fat intake correlated with more changes than protein and sucrose intake combined, pointing to fat intake independent of weight gain as a key determinant for metabolic regulation.

Because dietary long chain fatty acids, protein and simple carbohydrates are digested in the small intestine, particularly in jejunum, we hypothesized that diet-induced jejunal immune alterations might orchestrate subsequent host responses of glucoregulatory origin. In support of this hypothesis, HFD-induced intestinal *Tnfa* expression precedes both obesity and insulin resistance [50], while gut anti-inflammatory agents protect against insulin resistance, but not obesity [13]. Moreover, our multivariate analysis revealed that the expression of

several jejunal inflammatory gene transcripts correlated with expression of jejunal gluconeogenic gene transcripts.

Despite a similar reduction in glucose tolerance across all three HFDs examined, our data suggest that background diet, in this case protein:carbohydrate ratio, may have affected the 'route of action'. Both serum adiponectin and ACC phosphorylation in iWAT were diminished in HFHP and HFIP-fed mice compared to LFD reference mice, while HFNP-fed mice were less affected. In contrast, HFNP-fed mice had decreased adipose insulin signaling, as determined by AKT phosphorylation, compared to the LFD reference group, and increased NAFLD activity score compared to the HFIP and HFHP fed mice. HFIP-fed mice had a reduced abundance of OTUs belonging to the bacterial family S24-7 compared to any of the tested diets. Furthermore, Spearman correlation analyses showed that both dietary protein and fat but not sucrose negatively correlated with serum adiponectin levels. This is of particular interest since low carbohydrate intake counterbalanced by a high intake of protein and fat is a popular tool in weight losing regimes.

One limitation of the current study is the relative low n size in several of the experiments. Obviously, this affected the statistical power in the subsequent analysis of the data, and thereby may have promoted type 2 errors and the risk of accepting differences as non-significant. Nonetheless, the unique experimental settings applied in this study have enabled us to decipher how diets high in fat affect whole-body glucose homeostasis in mice independent of a confounding weight gain. The detailed physiological assessment of whole-body insulin sensitivity and tissue-specific glucose uptake, as well as comprehensive biochemical and histological analyses of a wide range of tissues and cell types, have provided us with valuable data that support a role of dietary fat *per se* to increase the gluconeogenic potential of intestinal epithelial cells, to contribute to development of glucose intolerance, and to decrease insulin-stimulated glucose uptake in adipose tissue. To our knowledge, no human studies have been conducted in which these effects of dietary fat have been investigated in the absence of a confounding weight gain. Results from such studies would be very interesting and obviously important for proper dietary guidance of people in need of maintaining or losing weight.

Author Contributions

A. Experimental conception and design: BAHJ, JTT, KB, LM, KK.
B. Data collection, analysis and interpretation: BAHJ, TSN, AMF, JBH, EF, AKS, SR, SIP, IS, AP, MP, TM, CS, BK, LM, KK, JTT.
C. Drafting the manuscript: BAHJ, KK, JTT.
D. Editing, revision and approval of final manuscript: All.

Financial support

Support for this study was provided by the Novo Nordisk Foundation Center for Basic Metabolic Research (CBMR). CBMR is an independent Research Center at the University of Copenhagen that is partially funded by an unrestricted donation from the Novo Nordisk Foundation (www.metabol.ku.dk).

Conflicts of Interest

The authors declare no conflicts of interest.

Acknowledgements

The authors would like to acknowledge Marianne Møller Andersen (Novo Nordisk Foundation Center for Basic Metabolic Research, University of Copenhagen) and Heidi Schlichting (University Hospital Schleswig-Holstein) for excellent technical assistance, and Bo Schmidt (University of Copenhagen) for statistical guidance.

Appendix A. Supplementary Data

Supplementary data to this article can be found online at http://dx.doi.org/10.1016/j.metabol.2016.09.002.

REFERENCES

[1] Ma T, Liaset B, Hao Q, Petersen RK, Fjære E, Ngo HT, et al. Sucrose counteracts the anti-inflammatory effect of fish oil in adipose tissue and increases obesity development in mice. PLoS One 2011;6:e21647. http://dx.doi.org/10.1371/journal.pone.0021647.
[2] Brøns C, Jensen CB, Storgaard H, Hiscock NJ, White A, Appel JS, et al. Impact of short-term high-fat feeding on glucose and insulin metabolism in young healthy men. J Physiol 2009;587:2387–97. http://dx.doi.org/10.1113/jphysiol.2009.169078.
[3] Turner N, Kowalski GM, Leslie SJ, Risis S, Yang C, Lee-Young RS, et al. Distinct patterns of tissue-specific lipid accumulation during the induction of insulin resistance in mice by high-fat feeding. Diabetologia 2013;56:1638–48. http://dx.doi.org/10.1007/s00125-013-2913-1.
[4] Hao Q, Lillefosse HH, Fjaere E, Myrmel LS, Midtbo LK, Jarlsby RH, et al. High-glycemic index carbohydrates abrogate the antiobesity effect of fish oil in mice. AJP Endocrinol Metab 2012;302:E1097–112. http://dx.doi.org/10.1152/ajpendo.00524.2011.
[5] Guilherme A, Virbasius JV, Puri V, Czech MP. Adipocyte dysfunctions linking obesity to insulin resistance and type 2 diabetes. Nat Rev Mol Cell Biol 2008;9:367–77. http://dx.doi.org/10.1038/nrm2391.
[6] Winer DA, Winer S, Shen L, Wadia PP, Yantha J, Paltser G, et al. B cells promote insulin resistance through modulation of T cells and production of pathogenic IgG antibodies. Nat Med 2011;17:610–7. http://dx.doi.org/10.1038/nm.2353.
[7] Lee YS, Li P, Huh JY, Hwang IJ, Lu M, Kim JI, et al. Inflammation is necessary for long-term but not short-term high-fat diet-induced insulin resistance. Diabetes 2011;60:2474–83. http://dx.doi.org/10.2337/db11-0194.
[8] Deng T, Lyon CJ, Minze LJ, Lin J, Zou J, Liu JZ, et al. Class II major histocompatibility complex plays an essential role in obesity-induced adipose inflammation. Cell Metab 2013;17:411–22. http://dx.doi.org/10.1016/j.cmet.2013.02.009.
[9] Nishimura S, Manabe I, Nagasaki M, Eto K, Yamashita H, Ohsugi M, et al. CD8+ effector T cells contribute to macrophage recruitment and adipose tissue inflammation in obesity. Nat Med 2009;15:914–20. http://dx.doi.org/10.1038/nm.1964.
[10] Lam YY, Ha CWY, Hoffmann JMA, Oscarsson J, Dinudom A, Mather TJ, et al. Effects of dietary fat profile on gut permeability and microbiota and their relationships with

metabolic changes in mice. Obesity 2015;23:1429–39. http://dx.doi.org/10.1002/oby.21122.
[11] Gruber L, Kisling S, Lichti P, Martin FP, May S, Klingenspor M, et al. High fat diet accelerates pathogenesis of murine Crohn's disease-like ileitis independently of obesity. PLoS One 2013;8:1–13. http://dx.doi.org/10.1371/journal.pone.0071661.
[12] Winer DA, Luck H, Tsai S, Winer S. The intestinal immune system in obesity and insulin resistance. Cell Metab 2016;1–14. http://dx.doi.org/10.1016/j.cmet.2016.01.003.
[13] Luck H, Tsai S, Winer S, Winer DAA, Revelo XSS, Lei H, et al. Regulation of obesity-related insulin resistance with gut anti-inflammatory agents. Cell Metab 2015;21:527–42. http://dx.doi.org/10.1016/j.cmet.2015.03.001.
[14] Ussar S, Griffin NW, Bezy O, Fujisaka S, Vienberg S, Softic S, et al. Interactions between gut microbiota, host genetics and diet modulate the predisposition to obesity and metabolic syndrome. Cell Metab 2015;22:516–30. http://dx.doi.org/10.1016/j.cmet.2015.07.007.
[15] Ayala JE, Bracy DP, Mcguinness OP, Wasserman DH. Considerations in the design of hyperinsulinemic–euglycemic clamps in the conscious mouse. Diabetes 2006;55:390–7. http://dx.doi.org/10.2337/diabetes.55.02.06.db05-0686.
[16] Ferré P, Leturque A, Burnol AF, Penicaud L, Girard J. A method to quantify glucose utilization in vivo in skeletal muscle and white adipose tissue of the anaesthetized rat. Biochem J 1985;228:103–10.
[17] Brandauer J, Andersen MA, Kellezi H, Risis S, Frøsig C, Vienberg SG, et al. AMP-activated protein kinase controls exercise training- and AICAR-induced increases in SIRT3 and MnSOD. Front Physiol 2015;6:85. http://dx.doi.org/10.3389/fphys.2015.00085.
[18] Larsson E, Tremaroli V, Lee YS, Koren O, Nookaew I, Fricker A, et al. Analysis of gut microbial regulation of host gene expression along the length of the gut and regulation of gut microbial ecology through MyD88. Gut 2012;61:1124–31. http://dx.doi.org/10.1136/gutjnl-2011-301104.
[19] Perreault N, Beaulieu JF. 27. Primary cultures of fully differentiated and pure human intestinal epithelial cells. Exp Cell Res 1998;245:34–42. http://dx.doi.org/10.1006/excr.1998.4221.
[20] Nik AM, Carlsson P. Separation of intact intestinal epithelium from mesenchyme. Biotechniques 2013;55:42–4. http://dx.doi.org/10.2144/000114055.
[21] Holm JB, Sorobetea D, Kiilerich P, Ramayo-Caldas Y, Estellé J, Ma T, et al. Chronic Trichuris muris infection decreases diversity of the intestinal microbiota and concomitantly increases the abundance of lactobacilli. PLoS One 2015;10:e0125495. http://dx.doi.org/10.1371/journal.pone.0125495.
[22] Caporaso JG, Kuczynski J, Stombaugh J, Bittinger K, Bushman FD, Costello EK, et al. QIIME allows analysis of high-throughput community sequencing data. Nat Methods 2010;7:335–6. http://dx.doi.org/10.1038/nmeth.f.303.
[23] Edgar RC, Haas BJ, Clemente JC, Quince C, Knight R. UCHIME improves sensitivity and speed of chimera detection. Bioinformatics 2011;27:2194–200. http://dx.doi.org/10.1093/bioinformatics/btr381.
[24] Edgar RC. Search and clustering orders of magnitude faster than BLAST. Bioinformatics 2010;26:2460–1. http://dx.doi.org/10.1093/bioinformatics/btq461.
[25] Wang Q, Garrity GM, Tiedje JM, Cole JR. Naive Bayesian classifier for rapid assignment of rRNA sequences into the new bacterial taxonomy. Appl Environ Microbiol 2007;73:5261–7. http://dx.doi.org/10.1128/AEM.00062-07.
[26] DeSantis TZ, Hugenholtz P, Larsen N, Rojas M, Brodie EL, Keller K, et al. Greengenes, a chimera-checked 16S rRNA gene database and workbench compatible with ARB. Appl Environ Microbiol 2006;72:5069–72. http://dx.doi.org/10.1128/AEM.03006-05.
[27] McMurdie PJ, Holmes S. Phyloseq: an R package for reproducible interactive analysis and graphics of microbiome census data. PLoS One 2013;8:e61217. http://dx.doi.org/10.1371/journal.pone.0061217.
[28] Paulson JN, Stine OC, Bravo HC, Pop M. Differential abundance analysis for microbial marker-gene surveys. Nat Methods 2013;10:1200–2. http://dx.doi.org/10.1038/nmeth.2658.
[29] Oksanen J, Blanchet FG, Kindt R, Legendre P, Minchin PR, O'Hara RB, et al. Vegan: community ecology package. R package version 2.3-3; 2016.
[30] Kleiner DE, Brunt EM, Van Natta M, Behling C, Contos MJ, Cummings OW, et al. Design and validation of a histological scoring system for nonalcoholic fatty liver disease. Hepatology 2005;41:1313–21. http://dx.doi.org/10.1002/hep.20701.
[31] Folch J, Lees M, Sloane Stanley GH. A simple method for the isolation and purification of total lipides from animal tissues. J Biol Chem 1957;226:497–509.
[32] Høeg LD, Sjøberg KA, Jeppesen J, Jensen TE, Frøsig C, Birk JB, et al. Lipid-induced insulin resistance affects women less. Diabetes 2011:60. http://dx.doi.org/10.2337/db10-0698.L.D.H.
[33] Mithieux G, Bady I, Gautier A, Croset M, Rajas F, Zitoun C. Induction of control genes in intestinal gluconeogenesis is sequential during fasting and maximal in diabetes. Am J Physiol Endocrinol Metab 2004;286:E370–5. http://dx.doi.org/10.1152/ajpendo.00299.2003.
[34] Croset M, Rajas F, Zitoun C, Hurot JM, Montano S, Mithieux G. Rat small intestine is an insulin sensitive gluconeogenic organ. Diabetes 2001;50:740–6. http://dx.doi.org/10.2337/diabetes.50.4.740.
[35] Mithieux G. A novel function of intestinal gluconeogenesis: central signaling in glucose and energy homeostasis. Nutrition 2009;25:881–4. http://dx.doi.org/10.1016/j.nut.2009.06.010.
[36] Mithieux G, Misery P, Magnan C, Pillot B, Gautier-Stein A, Bernard C, et al. Portal sensing of intestinal gluconeogenesis is a mechanistic link in the diminution of food intake induced by diet protein. Cell Metab 2005;2:321–9. http://dx.doi.org/10.1016/j.cmet.2005.09.010.
[37] Yu Y, Sitaraman S, Gewirtz AT. Intestinal epithelial cell regulation of mucosal inflammation. Immunol Res 2004;29:55–68. http://dx.doi.org/10.1385/IR:29:1–3:055 [IR:29:1–3:055 [pii]\r].
[38] Scheja L, Heese B, Zitzer H, Michael MD, Siesky AM, Pospisil H, et al. Acute-phase serum amyloid A as a marker of insulin resistance in mice. Exp Diabetes Res 2008;2008:230837. http://dx.doi.org/10.1155/2008/230837.
[39] Ruderman NB, Carling D, Prentki M, Cacicedo JM. Science in medicine AMPK, insulin resistance, and the metabolic syndrome. J Clin Invest 2013;123:2764–72. http://dx.doi.org/10.1172/JCI67227.2764.
[40] Hardie DG, FA R, SA H. AMPK: a nutrient and energy sensor that maintains energy homeostasis. Nat Rev Mol Cell Biol 2012;13:251–62. http://dx.doi.org/10.1038/nrm3311.
[41] Fritzen AM, Lundsgaard AM, Jordy AB, Poulsen SK, Stender S, Pilegaard H, et al. New nordic diet-induced weight loss is accompanied by changes in metabolism and AMPK signaling in adipose tissue. J Clin Endocrinol Metab 2015;100:3509–19. http://dx.doi.org/10.1210/jc.2015-2079.
[42] Lihn AS, Pedersen SB, Richelsen B. Adiponectin: action, regulation and association to insulin sensitivity. Obes Rev 2005;6:13–21. http://dx.doi.org/10.1111/j.1467-789X.2005.00159.x.
[43] Fu Y, Luo N, Klein RL, Garvey WT. Adiponectin promotes adipocyte differentiation, insulin sensitivity, and lipid accumulation. J Lipid Res 2005;46:1369–79. http://dx.doi.org/10.1194/jlr.M400373-JLR200.
[44] Wu X, Motoshima H, Mahadev K, Stalker TJ, Scalia R, Goldstein BJ. Involvement of AMP-activated protein kinase in glucose uptake stimulated by the globular

domain of adiponectin in primary rat adipocytes. Diabetes 2003;52:1355–63. http://dx.doi.org/10.2337/diabetes.52.6.1355.

[45] Degawa-Yamauchi M, Moss KA, Bovenkerk JE, Shankar SS, Morrison CL, Lelliott CJ, et al. Regulation of adiponectin expression in human adipocytes: effects of adiposity, glucocorticoids, and tumor necrosis factor alpha. Obes Res 2005;13:662–9. http://dx.doi.org/10.1038/oby.2005.74.

[46] Hasegawa G, Ohta M, Ichida Y, Obayashi H, Shigeta M, Yamasaki M, et al. Increased serum resistin levels in patients with type 2 diabetes are not linked with markers of insulin resistance and adiposity. Acta Diabetol 2005;42:104–9. http://dx.doi.org/10.1007/s00592-005-0187-x.

[47] Sajadi SMA, Khoramdelazad H, Hassanshahi G, Rafatpanah H, Hosseini J, Mahmoodi M, et al. Plasma levels of CXCL1 (GRO-alpha) and CXCL10 (IP-10) are elevated in type 2 diabetic patients: evidence for the involvement of inflammation and angiogenesis/angiostasis in this disease state. Clin Lab 2013;59:133–7.

[48] van Exel E, Gussekloo J, de Craen AJM, Frölich M, Bootsma-Van Der Wiel A, Westendorp RGJ, et al. Low production capacity of interleukin-10 associates with the metabolic syndrome and type 2 diabetes: the Leiden 85-Plus study. Diabetes 2002;51:1088–92.

[49] Kiilerich P, Myrmel LS, Fjære E, Hao Q, Hugenholz F, Sonne SB, et al. Effect of a long-term high-protein diet on survival, obesity development and gut microbiota in mice. Am J Physiol Endocrinol Metab 2016. http://dx.doi.org/10.1152/ajpendo.00363.2015.

[50] Ding S, Chi MM, Scull BP, Rigby R, Schwerbrock NMJ, Magness S, et al. High-fat diet: bacteria interactions promote intestinal inflammation which precedes and correlates with obesity and insulin resistance in mouse. PLoS One 2010;5:e12191. http://dx.doi.org/10.1371/journal.pone.0012191.